

**Dispersion of hydroxyapatite nanoparticles in solution and
in polycaprolactone composite scaffolds**

Journal:	<i>Journal of Materials Chemistry B</i>
Manuscript ID	TB-ART-10-2015-002255.R1
Article Type:	Paper
Date Submitted by the Author:	04-Dec-2015
Complete List of Authors:	Goonasekera, Chandhi; The University of Queensland, Australian Institute for Bioengineering and Nanotechnology; The University of Queensland, Australian Institute for Bioengineering and Nanotechnology (AIBN) Jack, Kevin; The University of Queensland, Australian Institute for Bioengineering and Nanotechnology Cooper-White, Justin; The University of Queensland, Australian Institute for Bioengineering and Nanotechnology (AIBN) Grondahl, Lisbeth; The University of Queensland, School of Chemistry and Molecular Biosciences

Dispersion of hydroxyapatite nanoparticles in solution and in polycaprolactone composite scaffolds

Chandhi S. Goonasekera,^{†,‡,#} Kevin S. Jack,^{‡,*} Justin J. Cooper-White,^{#,^,\$,*} Lisbeth Grøndahl^{†,*}

[†]School of Chemistry and Molecular Biosciences, The University of Queensland, St. Lucia, QLD 4072, Australia

[‡]Centre for Microscopy and Microanalysis, The University of Queensland, St. Lucia, QLD 4072, Australia

[#] Tissue Engineering and Microfluidics Laboratory, Australian Institute for Bioengineering and Nanotechnology, The University of Queensland, St. Lucia 4072 Australia

[^]The School of Chemical Engineering, The University of Queensland, St. Lucia 4072 Australia

^{\$}CSIRO, Division of Materials Science and Engineering, Clayton, Victoria 3169 Australia

**Corresponding Authors:*

Associate Professor Lisbeth Grøndahl

Phone: +61 7 336 53671 Fax: +61 7 336 54299 Email: l.grondahl@uq.edu.au

Professor Justin J Cooper-White

Phone: +61 7 334 63858 Email: j.cooperwhite@uq.edu.au

Dr Kevin Jack

Phone: +61 7 33651143 Email: k.jack@uq.edu.au

ABSTRACT

The dispersion behaviour of hydroxyapatite nanoparticles (HAP) and surface-modified HAP was studied in 1,4-dioxane (DO), water and poly(ϵ -caprolactone) (PCL) solutions and the relationship between these and the dispersion in composite PCL scaffolds prepared by thermally induced phase separation (TIPS) was examined. Investigation of the change in particle sizes by dynamic light scattering, showed that the modification of HAP by adsorption or covalent attachment of heparin via a 3-aminopropyltriethoxysilane (APTES) layer improved the dispersion stability of the particles in water/DO mixtures, while no improvement was observed in DO. The distribution of the particles within the composite scaffolds was determined using a combination of transmission electron microscopy and a calcium quantification method which was used to determine distribution of the particles in the vertical direction. While the scaffolds fabricated in DO had particles embedded within the walls of the scaffold, the scaffolds fabricated in a DO/water mixed solvent showed the particles partitioned to the surface of the scaffold walls, which is likely because the particles acted as interface stabilisers and were not miscible with the PCL rich phase. Therefore, it can be concluded that the polymer-solvent system used, as well as the phase separation mechanism that occurs, significantly influences the distribution of the particles in the scaffolds and thus the particle behaviour in solution is not necessarily a good predictor for the ability to fabricate scaffolds with a high degree of particle dispersion and hence for overall materials performance. Bulk crystallinity and compressive modulus were examined and it was determined that no significant changes occurred compared with the pristine PCL, while the surface bioactivity of the scaffolds had improved significantly, indicating that the particles were present at the polymer-solution interface.

INTRODUCTION

Nanosized hydroxyapatite has previously been incorporated in thermoplastic polyesters composites to improve both the mechanical strength and the bioactivity of the polymer.¹⁻³ Schaefer and Justice demonstrated, using ultra-small-angle scattering techniques, that micron-scale aggregation of nanoparticles present in composites reduced the ability of the particles to reinforce the material,⁴ and this can be attributed to the aggregates acting as stress initiators and stress concentrators that initiate the failure of the construct.⁵ Several studies on non-porous composites have shown that the degree of aggregation can be reduced by modifying the surface of the hydroxyapatite,⁶⁻¹³ so as to improve the colloidal stability of the particles in the precursor polymer solutions with the aim of creating well-dispersed particles in the final construct. To this end, a number of investigations have reported improvements in the colloidal stability of hydroxyapatite in various solvents after surface

modification through visual observations of the suspensions over time,^{7, 10, 14-16} investigating the sedimentation volume,^{17, 18} and from measurements of the zeta potential.¹⁶⁻¹⁸ Based on a previous study which showed that heparin, when adsorbed onto hydroxyapatite, can improve the dispersion of the particles in a number of solvents,⁹ we recently reported the synthesis and characterisation of a series of heparin-modified hydroxyapatite particles (heparin adsorbed or covalently linked) which displayed zeta potentials in 1 mM KCl that were dependent on the mode of heparin attachment.¹⁹

The properties of a composite scaffold are governed by the collective properties of the filler particle (surface chemistry, mechanical properties and particle size), the polymer (functional groups, crystallinity and molecular weight) and the resultant interface (interfacial strength and dispersion achieved).²⁰ In porous composite scaffolds, most investigations to-date have incorporated unmodified hydroxyapatite particles,^{1, 3, 21-26} with only a limited number of studies having investigated the effect of hydroxyapatite surface modification on the properties of the scaffolds.^{2, 27-29} For example, it was reported that the incorporation of γ -methacryloxypropyltrimethoxysilane-modified hydroxyapatite into poly(L-lactic acid) (PLLA) scaffolds resulted in compressive moduli at least 30% higher than that of pristine hydroxyapatite composite scaffolds, at particle loadings of 20 - 30 wt%.²⁷ Moreover, from a study of the reinforcement of poly(ϵ -caprolactone) PCL composite scaffolds with PCL grafted hydroxyapatite it was observed that the compressive modulus of a scaffold incorporating 20 wt% of grafted hydroxyapatite was 59 % greater than the composite scaffold containing the same loading of pristine hydroxyapatite.²⁸ While these works represent clear indications that modified hydroxyapatite can significantly enhance scaffold performance, there is limited knowledge of the level of distribution of the nano-sized particles in the porous, three-dimensional composite scaffolds.

A major challenge in probing the nanoparticle distribution in porous composites is the shortage of analytical tools that have the required resolution and dynamic range to simultaneously identify aggregation and distribution of particles against a porous background and in three dimensions. Techniques such as scanning electron microscopy-energy dispersive x-ray spectroscopy (SEM-EDX) have been used to determine that HAP is distributed throughout a composite,³⁰ and can be used to identify micron-sized particle aggregates.¹ Transmission electron microscopy (TEM) has been utilised to evaluate the dispersion of HAP in a scaffold,^{27, 31} however, the technique is inherently two-dimensional. Other methods that may be used to give information on the nano-scale include time-of-flight secondary-ion mass spectrometry (ToF-SIMS) surface imaging and small-angle scattering methods,³² but each of these methods has its own inherent limitations; e.g. a lack of three-dimensional information in the case of ToF-SIMS³³ and the complexity of modelling required to interpret the Fourier space images afforded by scattering methods. It is also noted that nano-CT

has demonstrated some applicability for characterising nano-composite scaffolds,³⁴ however, it is still to be fully developed.

Bulk characterisation methods can alternatively be used to indirectly evaluate the dispersion and strength of interfacial interactions and include mechanical properties and polymer crystallinity. The dispersion of a filler in a polymer matrix is affected by a number of parameters including the flexibility of the polymer chains, the ability for the chains to crystallise, the functional groups present and molecular weight.³⁵ Moreover, the conformation and viscoelasticity of the polymer chains adsorbed to the particles' surface are altered depending on the extent of attractive interactions at the interface.³⁶ The presence of nanoparticles can affect the crystallinity (X_c) of a polymer by acting as nucleation sites for the growth of polymer crystallite.^{11, 12, 28, 37} The presence of well-dispersed particles which provide a large interfacial area is necessary to induce the formation of a transcrystalline layer³⁸ and the presence of such layers has been linked to enhanced mechanical properties, due to the stronger bonding between the filler particle and polymer matrix.^{2, 28}

While the dispersion of hydroxyapatite particles within the polymer matrix is a requirement for reinforcement of a scaffold, the presentation of the particles at the surface of the scaffold walls is also of key importance because it improves the bioactivity of the scaffold. This aspect has been typically evaluated through the deposition of apatite from simulated body fluid (SBF) *in vitro*^{1, 23, 24} as this simple test has been shown to correlate with bone bonding activity *in vivo*.³⁹ The inclusion of hydroxyapatite has been observed to increase the adsorption of protein to scaffolds,^{3, 21, 27} and it has been found to enhance the attachment and proliferation of osteoblasts and osteoblast-like cells.^{2, 3, 22, 25, 40} This enhanced biological activity has been attributed to the highly bioactive nature of hydroxyapatite providing a nucleation point for further mineralisation as well as an anchor point for osteoblasts mediated by the adsorbed protein layer. In addition, some studies have proposed additional effects including the surface presentation of hydroxyapatite creating a nano-textured surface roughness as well as the dissolution of hydroxyapatite leading to the formation of a crystalline carbonated calcium phosphate layer, which is incorporated into the bone collagenous matrix.^{2, 41, 42}

The overall aim of this study is to investigate the dispersion of a series of heparin-modified hydroxyapatite particles both in solution and in composite scaffolds. The dispersion of the particles was investigated using dynamic light scattering (DLS) in aqueous solutions, dioxane (DO), a mixed DO/water solvent, and PCL solutions. Composite PCL scaffolds were fabricated using the thermally induced phase separation (TIPS) method using different solvent systems and cooling

regimes. The distribution of the particles within the scaffolds was determined using a combination of SEM and TEM (to evaluate agglomeration and dispersion within the polymer) and a calcium quantification (to determine distribution of the particles in the vertical direction). The formation of apatite on the scaffolds was assessed by immersion in SBF. In addition, bulk materials properties such as the degree of crystallinity and compressive moduli were investigated.

MATERIALS AND METHODS

Materials

The fabrication of hydroxyapatite nanoparticles (HAP) and 3-aminopropyltriethoxysilane (APTES) modified particles cured for 24 hours at 150 °C (A-HAP) were carried out as described in our previous publication.⁴³ Two types of particles incorporating heparin either adsorbed onto HAP, to generate HEP-HAP, or covalently linked to the amine groups of A-HAP to form HEP-A-HAP were fabricated as previously described¹⁹. Poly(ϵ -caprolactone) (PCL) (M_n of 70000 - 90000 g mol⁻¹, density 1.145 g cm⁻³) was purchased from Sigma-Aldrich. DO (assay 99.8 %) was obtained from Lab-Scan Analytical Sciences, dried over molecular sieves and filtered twice through a 0.2 μ m mesh-size hydrophobic PTFE syringe filter prior to use. Isopropanol was obtained from Merck. Simulated body fluid (SBF) was made from the following high-purity salts: KCl (purity \geq 99.5 %) from Merck, NaCl (purity \geq 99.9 %), NaHCO₃ (purity \geq 99.7 %), Na₂SO₄ (purity \geq 99.0 %) and conc. HCl (32 % (w/w), minimum assay 31.5 %) from Univar, MgCl₂.6H₂O (purity \geq 99.0 %), CaCl₂ (purity \geq 93.0 %) from Chem-Supply, NaOH pellets (purity 97.0 %) from Pronalys, tris-hydroxymethyl aminomethane (Tris) (purity \geq 99.8%) from Spectrum and K₂HPO₄.3H₂O (purity \geq 99.0 %) was purchased from Sigma-Aldrich. Deionized water (Milli-Q) water was used for preparation of all aqueous solutions.

Preparation of particle suspensions

Suspensions of HAP, A-HAP, HEP-HAP and HEP-A-HAP, at a concentration of 0.50 g L⁻¹, were prepared in DO or 1 mM KCl by sonicating the dry, finely ground particles in DO or 1 mM KCl for 30 seconds. Serial dilution was used to make a series of suspensions containing 0.25 g L⁻¹, 0.13 g L⁻¹, 0.06 g L⁻¹ and 0.03 g L⁻¹ of each particle type.

HEP-HAP and HEP-A-HAP suspensions (0.1, 0.5 and 1.0 g L⁻¹) were prepared in 5 % (v/v) water/DO solution by sonicating 1, 5 and 10 mg of the dry, finely ground sample in 0.5 mL water, then adding 9.5 mL DO and sonicating the suspension again for 5 minutes.

A solution of PCL was prepared by dissolving 5.00 g of PCL in 95 mL of DO overnight at room temperature. Dry, finely ground HEP-HAP and HEP-A-HAP (sample masses ranging from 1 - 40 mg) was dispersed in 0.5 mL water or 0.5 mL 1 mM KCl by sonication for 2 minutes and 9.5 mL of the prepared PCL solution was added. This mixture was stirred for 10 minutes to redissolve any PCL that had precipitated out and to homogenise the mixture and the mixture was further sonicated for 5 minutes.

Fabrication of PCL scaffolds from DO solution

PCL (5.00 g) was dissolved in 100 mL of DO overnight at room temperature to obtain a 50 g L⁻¹ solution. When the polymer had dissolved (observed by the solution turning clear, typically within 15 hours), 3 mL of the solution was transferred to a glass test-tube with an internal diameter of 8 mm. The tube was capped and sealed with para-film and was then maintained at 22 °C for 10 minutes in an ethylene glycol bath and then cooled at a rate of 0.5 °C min⁻¹ down to -10 °C. After the resultant scaffolds were frozen, the glass mould was broken and the scaffolds immediately placed in a vacuum chamber to sublime the DO. Depressurization of the chamber was conducted using a turbo-molecular pump until the internal pressure of the chamber was in the range of 10⁻⁸ bar. Any remaining DO in the scaffolds was leached out by first wetting the scaffolds with isopropanol for 30 seconds and then washing in water overnight at room temperature. Finally, the PCL_{DO-S} scaffolds obtained were air-dried at room temperature before being placed in a desiccator to remove any remaining water.

Fabrication of PCL scaffolds from water/DO solution

PCL (5.00 g) was dissolved in 95 mL of DO overnight at room temperature, followed by the addition of 5 mL of water to obtain a 50 g L⁻¹ PCL solution in 5 % (v/v) water/DO. The mixture was stirred for 10 minutes to homogenise and redissolve any PCL that had precipitated upon the addition of the water. 3 mL of the solution was transferred to a glass test-tube and treated in the same manner as outlined in Section 2.3, to obtain PCL_{DO-H₂O-S} scaffolds. The procedure was

repeated with the cooling step being changed to a fast quenching step in which the test-tube with the PCL solution was placed in a $-18\text{ }^{\circ}\text{C}$ freezer for 1 hour, to fabricate $\text{PCL}_{\text{DO-H}_2\text{O-Q}}$ scaffolds.

Fabrication of PCL composite scaffolds

Composite scaffolds were prepared using HAP, A-HAP, HEP-HAP and HEP-A-HAP. 40 mg of dry, finely ground particles was dispersed in 10 mL of the 50 g L^{-1} PCL solution in DO, by sonication for 5 minutes, to obtain 4 mg mL^{-1} suspensions. 3 mL of this suspension was transferred to a glass test tube and treated in the same manner as outlined in Section 2.3 to obtain $x\text{-PCL}_{\text{DO-S}}$ scaffolds, where x refers to the type of particle incorporated e.g. HAP- $\text{PCL}_{\text{DO-S}}$ scaffolds contained unmodified HAP particles. In order to incorporate the particles in $\text{PCL}_{\text{DO-H}_2\text{O-S}}$ and $\text{PCL}_{\text{DO-H}_2\text{O-Q}}$ scaffolds, 5.00 g of PCL was dissolved in 95 mL DO at room temperature overnight. 40 mg of the particles was dispersed in 0.5 mL water, by sonication for 2 minutes and 9.5 mL of the prepared PCL solution was added to obtain 4 mg mL^{-1} suspensions. This mixture was stirred for 10 minutes to redissolve any PCL that had precipitated out and to homogenise the mixture. The mixture was then sonicated for 5 minutes and 3 mL was transferred into a glass test tube and treated in the same manner as outlined in Section 2.4, to obtain $x\text{-PCL}_{\text{DO-H}_2\text{O-S}}$ and $x\text{-PCL}_{\text{DO-H}_2\text{O-Q}}$ scaffolds.

Characterization

A Mettler Toledo TGA/DSC 1 STAR^e system was used to determine the percentage of inorganic and organic constituents. Approximately 10 - 15 mg of sample was placed in an aluminium crucible and heated at a rate of $10\text{ }^{\circ}\text{C min}^{-1}$ from $25\text{ }^{\circ}\text{C}$ to $600\text{ }^{\circ}\text{C}$. Controls of pure PCL and pristine HAP were run to determine inherent mass loss.

The elemental composition of the sample surface was measured with a Kratos Axis ULTRA X-ray photoelectron spectrometer using a monochromated Al K_{α} (1486.6 eV) anode source operating at 15 kV and 10 mA (150 W). Survey (wide) scans of the sample were taken with a pass energy of 160 eV over a binding energy range of 550 - 50 eV with 0.2 eV steps and a dwell time of 100 ms. The atomic concentrations were determined by deconvolution of the resulting spectra using a least-squares optimisation routine in the CasaXPS software.

The hydrodynamic diameters of the particles were measured using a Malvern Zetasizer 3000HS instrument. The size measurements of particles in suspensions were conducted in glass cells at $25\text{ }^{\circ}\text{C}$. Each measurement consisted of the sum of at least 5 co-added correlation plots and the final

value obtained was taken from the average of three replicate measurements. The hydrodynamic radii determined in this method represent a mean spherical diameter of the particles or aggregates; although the primary particles are elongated in nature as described below.

Sedimentation studies were conducted by placing 10 mL of the particle suspensions in pre-weighed vials of 57 mm height and 27 mm diameter. In each suspension, the height of the suspension meniscus was at 2.2 cm from the bottom of the vial. The suspensions were allowed to stand for a period of 2 hours, after which the supernatant was carefully removed using a glass pipette, so as not to disturb the sediment (~3 - 5 mm of suspension remained). The dried residue was weighed and subjected to TGA as described above.

The distribution of particles in the polymer walls of the scaffold was determined using a JEOL 1010 TEM microscope operating at an accelerating voltage of 100 kV. TEM analysis was conducted on sections of the PCL scaffolds obtained at 0 - 5 mm, 15 - 20 mm and 30 - 35 mm from the bottom of the scaffold. Samples were prepared by placing them in 0.6 mL eppendorf tubes in an automated freeze substitution apparatus (AFS2, Leica) and Lowicryl resin was added at -20 °C. Samples were maintained at -20 °C for 4 hours before UV polymerisation of the resin, initially for 12 hours at -20 °C and then for 24 hours at 20 °C. The samples were then sectioned to a thickness of 100 nm on a UC6 ultramicrotome at using a 35° diamond knife (Diatome) and placed on formvar-coated slot grids for TEM analysis. In the TEM images of the polymer sections, the particles were segmented from the polymer background using the *Threshold* tool on ImageJ 1.44p software.⁴⁴ The boundaries of the polymer region were selected manually using the *Polygons selection* tool as illustrated in Supplementary Material Figures S1 and S2 and the percentage area of the polymer covered by the particles was calculated. The average area of 3 segmented images was considered for each sample.

SEM imaging of sections of the scaffolds was conducted on 3 mm thick sections obtained 15 - 20 mm from the bottom of each scaffold. The sections were coated with a 15 nm thick Pt coating in an argon atmosphere using a Baltec Ion Coater (15 mA, 150 s) to prevent charging during image acquisition. The sample morphology was studied using either a Philips XL30 or a JEOL JSM-6610 scanning electron microscope. Both microscopes use a LaB₆ filament which was operated at a 10 kV accelerating voltage and at a 10 mm working distance. The pore sizes of scaffolds were measured from SEM images of the cross sections of the scaffolds. ImageJ 1.44p software⁴⁴ was used to draw circles touching the pore walls, but completely enclosed within pores (as shown in Supplementary Figure S3) and the diameter of the circle was taken as the pore diameter. At least 40 pores were measured to determine the pore size range. The procedure was repeated to determine the size range of the micropores in the walls (Supplementary Figure S3).

The distribution of HAP in the scaffolds in the vertical direction was determined using 5 mm thick sections taken at a distance of 0 - 5, 5 - 10 and 30 - 35 mm from the bottom of the scaffolds. Each section was dissolved in 5 mL of toluene, followed by the addition of 10 mL of HCl solution at pH 1.7. The mixture was stirred for 10 minutes at room temperature and exposed to the atmosphere overnight to facilitate evaporation of the toluene. Afterwards, the remaining 'skin' of PCL left on top of the solution was removed and the volume of the solution was made up to 25 mL using MilliQ water. The pH of the solution was adjusted to between 3 and 4 using a saturated NaOH solution. The calcium concentration in each solution was determined using a ThermoScientific calcium combination ion-selective electrode (9720BNWP) and converted to the concentration of HAP assuming the stoichiometry of HAP to be $\text{Ca}_5(\text{PO}_4)_3\text{OH}$. Calibration of the electrode was conducted using calcium solutions of 100, 10 and 1 ppm Ca prepared from anhydrous CaCl_2 , by a serial dilution method. The pH of the standard solutions was adjusted to between 3 and 4 using conc. HCl. A two-point calibration was conducted on the electrode using the standard solutions and the concentration range measured of the samples was between 5 - 100 ppm of Ca.

The densities of the scaffold were estimated using 5 mm thick scaffold sections obtained from 5 - 10 mm from the bottom of the scaffolds. The diameter and the height of each section were measured using a Vernier Calliper to calculate the volume (V_{scaffold}) (assuming the scaffold section to be cylindrical). The mass of each section (m_{scaffold}) was measured using an analytical balance and the scaffold density (D_{scaffold}) calculated using Equation 1.

$$D_{\text{scaffold}} = \frac{m_{\text{scaffold}}}{V_{\text{scaffold}}} \quad (1)$$

In order to calculate the porosity (ϵ), the cumulative density of the starting materials PCL and HAP ($D_{\text{materials}}$) in the scaffold section was calculated using Equation 2.

$$D_{\text{materials}} = \frac{[X_H \rho_H + (1 - X_H) \rho_P] - D_{\text{scaffold}}}{[X_H \rho_H + (1 - X_H) \rho_P]} \times 100 \% \quad (2)$$

Where ρ_H is the density of HAP (3.156 g cm^{-3}),⁴⁵ ρ_P is the density of PCL (1.145 g cm^{-3})⁴⁶ and X_H is the mass fraction of HAP in the section determined by Ca ion selective electrode (see above). The porosity was then calculated using Equation 3.

$$\epsilon = \frac{D_{\text{materials}} - D_{\text{scaffold}}}{D_{\text{materials}}} \times 100\% \quad (3)$$

The average densities of 3 scaffold sections were used to determine the porosity of each type of scaffold.

The crystallinity of the PCL scaffolds was evaluated from differential scanning calorimeter data using a Mettler Toledo TGA/DSC 1 STAR^e system. Scaffold sections at 30 - 35 mm from the bottom were taken (5 - 7 mg) and were placed in aluminium pans, sealed and run at a heating/cooling rate of 10 °C min⁻¹. Samples underwent a 3 cycle run (from -100 to 100 °C; from 100 to -100 °C and from -100 to 100 °C). The measured enthalpy of melting (ΔH_m) was determined from each DSC trace using the data acquisition program Mettler STAR^e. The crystalline content (X_c) was determined from the first heating cycle, using Equation 4,

$$X_c = \frac{\Delta H_m}{\omega \times \Delta H_{m,100}} \quad (4)$$

Where ω is the weight fraction of PCL in the scaffold and $\Delta H_{m,100}$ is the enthalpy of melting of the 100% crystalline polymer. For PCL,⁴⁷ $\Delta H_{m,100}$ was taken to be 139.5 J g⁻¹.

Compression testing of sections of the scaffolds was conducted by immersion the scaffolds in liquid nitrogen for 5 minutes to facilitate the cutting of 5 mm sections at 5 - 10 mm from the bottom of the scaffold resulting in the test specimens with dimensions of 8 mm in width and 5 mm in height. The obtained sections were placed in a dessicator overnight to remove any condensed water before being subjected to compression testing. Compression testing was performed under ambient conditions using an INSTRON 5543 instrument with a 500 N load cell at a strain rate of 10 % min⁻¹, up to a 40 % compressive strain. The compressive modulus was determined using the slope of the stress-strain curve in the elastic region.

SBF was prepared as outlined by Kokubo et al.³⁹ Sections from 15 - 20 mm from the bottom of each scaffold were obtained as 5 × 5 × 5 mm³ cubes so that the outer skin of the scaffold was removed. The initial masses of these sections were measured using an analytical balance. These were immersed in 30 mL of SBF pre-warmed to 37.0 ± 0.5 °C in plastic tubes and placed in a water bath at 37.0 ± 0.5 °C. The SBF solution was changed every 3 days and after 13 days the scaffolds were removed from the solutions, rinsed with MilliQ water and left to dry in a dessicator and the samples were re-weighed to determine the percentage mass change.

Statistical analysis

The determination of the mass of particles sedimenting from suspensions was carried out once. All other experiments were carried out with 3 replicate samples, with the exception of compression testing experiments where 3 - 5 replicate samples were measured. Results are expressed as mean ±

standard deviation. Statistical analysis was done using a two-tailed student's *t* test. A probability of $p < 0.05$ was considered to be statistically significant.

RESULTS AND DISCUSSION

Behaviour of particles in suspension

The synthesis and chemical characterisation of the hydroxyapatite nano-particles used in the current study have previously been published.^{19, 43} The nano-particles include the as prepared particles, HAP, as well as APTES-modified particles, A-HAP, and two types of particles incorporating heparin; either adsorbed onto HAP (HEP-HAP) or covalently linked to the amine groups of A-HAP (HEP-A-HAP). The dry, finely ground hydroxyapatite nano-particles were dispersed in 1 mM KCl or DO solution at particle concentrations ranging from 0.03 to 0.50 g L⁻¹. The results of the measurements of particle size by DLS are shown in Figures 1 A and B. It was observed for dispersions in 1 mM KCl (Figure 1 A) that HAP and A-HAP particle diameters were larger than 1 μm , which is significantly larger than their primary particle sizes observed from TEM (lengths of particles were 180 ± 80 nm and 200 ± 60 nm for HAP and A-HAP, respectively⁴³), and indicates that the suspensions are largely comprised of aggregates. In contrast, the particle sizes observed for HEP-HAP and HEP-A-HAP were comparable to the primary particle sizes observed from TEM where the lengths of the particles were 170 ± 50 nm and 220 ± 60 nm for HEP-HAP and HEP-A-HAP, respectively.¹⁹ This is consistent with the higher zeta potentials reported for the particles modified with HEP in 1 mM KCl (i.e., -7.4 ± 0.2 , 3.0 ± 5.4 , -19.9 ± 0.4 , -23.0 ± 0.3 mV for HAP, A-HAP, HEP-HAP and HEP-A-HAP, respectively^{19, 43}) and demonstrates that the attachment of heparin to the HAP surface, regardless of the mode of attachment, was a successful method of improving colloidal stability in aqueous solution. This effect of heparin has been observed previously^{18, 48} and is attributed both to the electrostatic repulsion caused by the increased negative surface charge introduced by heparin and to steric repulsion due to the relatively large molecular weight of heparin.

The results for the suspensions in DO (Figure 1 B) show that HAP, A-HAP and HEP-HAP all display mean particle sizes larger than 1 μm at all concentrations. The HEP-A-HAP particles, however, had an average particle diameter of 450 nm at 0.03 g L⁻¹ and an increase in mean particle size with particle concentration was observed, reaching a particle size greater than 1 μm at 0.5 g L⁻¹. In addition, all of the dispersions studied here, with the exception of heparin-modified particles in aqueous suspensions, showed an increase in mean size with increasing concentration. The heparin-

modified particles in aqueous suspensions, in contrast, showed no significant change in mean particle size as a function of concentration of particles. The different behaviour of the heparin-modified particles in DO compared to water can be explained by the different physical properties of the non-polar DO and the hydrophilic heparin molecule (e.g., heparin is insoluble in methanol⁴⁹). It is, therefore, expected that the interactions between heparin and DO are limited to van der Waals' and dipole-induced-dipole interactions reducing both steric and electrostatic stabilisation.

DLS measurements were further performed on suspensions of particles containing 5 % (v/v) water in DO (water/DO). These DLS measurements were conducted on HEP-HAP and HEP-A-HAP suspensions at 0.1, 0.5 and 1.0 g L⁻¹ particle concentrations and are presented in Figure 1 C. This data show that the particle diameters of both particle types were less than 1 µm at all particle concentrations. An increase in particle size with increasing concentration was evident (statistically significant for HEP-HAP at 0.1 or 0.5 compared to 1 g L⁻¹). Based on this data it appears that the mode of heparin attachment did not affect the dispersion stability in water/DO. However, the particle sizes of both types of particles in water/DO (Figure 1 C) were significantly smaller compared to in DO (Figure 1 B) ($p = 0.05$ and 0.04 for HEP-HAP and $p = 0.03$ and < 0.01 for HEP-A-HAP at 0.1 g L⁻¹ and 0.5 g L⁻¹, respectively). Moreover, the HEP-HAP particles were significantly larger in water/DO (Figure 1 C) than in 1 mM KCl (Figure 1 A) at both 0.1 g L⁻¹ and 0.5 g L⁻¹ particle concentrations ($p < 0.01$ in both cases), but there was no significant difference between the particle sizes of HEP-A-HAP when dispersed in 1 mM KCl at 0.1 g L⁻¹ and 0.5 g L⁻¹ particle concentrations, compared to in water/DO ($p = 0.26$ and 0.07 , respectively). The level of dispersion of these two particles types can therefore be represented as: HEP-HAP dispersion increases from DO to water/DO to water, while HEP-A-HAP dispersion increases from DO to water/DO ~ water.

To better understand the behaviour of the suspensions used in the fabrication of scaffolds, DLS measurements of HEP-HAP and HEP-A-HAP were conducted for particle concentrations from 0.1 to 4.0 g L⁻¹ in 5% (v/v) water/DO solutions containing 50 g L⁻¹ of PCL (referred to here as PCL/water/DO) and the results are shown in Figure 1 D. At a particle concentration of 4.0 g L⁻¹ the particles were significantly larger than at 0.1 g L⁻¹ for both particle types. The particle sizes, however, for both types of particles were observed to be less than 1 µm at all particle concentrations. Similar behaviour was observed when the particles were suspended in a PCL/(1 mM KCl)/DO solution (1 mM KCl replacing water) as detailed in the Supplementary Materials Figure S4.

Fabrication and characterization of PCL TIPS scaffolds

Pure PCL scaffolds were fabricated using the TIPS method from 50 g L⁻¹ of PCL in either DO or 5 % (v/v) water/DO solutions. The phase separation behaviour of 50 g L⁻¹ PCL solutions was investigated and the details are provided in the Supplementary Materials (including Figure S5). Although an actual bimodal curve of the system could not be determined from these experiments due to the polydispersity of PCL,^{50, 51} the measurements were useful indicators of the temperatures at which the homogenous region and phase-separated region of the polymer solution could be distinguished.⁵⁰ The PCL/water/DO solutions that had 5 % (v/v) water underwent a liquid-liquid separation at -8 ± 1 °C, before freezing at -10 ± 1 °C. Solutions of PCL in DO did not have a cloud point, and froze (solid-liquid separation) at -4 ± 1 °C. This correlates with other studies which have shown that this mechanism of phase separation is favoured when DO is used as the solvent.⁵²⁻⁵⁴ The freezing temperature recorded was below that of the melting temperature of the pure solvent (11.8 °C) correlating with the polymer at the crystallization front causing constitutional supercooling.⁵⁵

For scaffold fabrication, two different freezing regimes were investigated, slow quench in which the temperature was decreased from 22°C to -10 °C, at a cooling rate of 0.5 °C min⁻¹ and quick quench in which the samples were cooled from room temperature to -18 °C in a freezer, and a total of three scaffold types were produced. Two scaffold types were produced using the slow quench method, i.e. PCL_{DO-S} and PCL_{DO-H2O-S}, while one scaffold type was produced using the quick quench method, i.e. PCL_{DO-H2O-Q}. SEM analysis of the scaffolds (see Figure 2), revealed that the architectures were significantly different in the different types of scaffolds. The pores of PCL_{DO-H2O-Q} were anisotropic and the pore sizes of these scaffolds were difficult to determine due to the lack of discrete pores as can be seen from the SEM image in Figure 2 A. The porosities of the PCL_{DO-S} and PCL_{DO-H2O-S} scaffolds were similar at $94 \pm 1\%$. The PCL_{DO-H2O-S} scaffold shown in Figure 2 B displayed a highly interconnected fibrous architecture where the scaffold pores were heterogeneous and isotropic with an estimated pore size of 3 - 50 µm. The PCL_{DO-S} scaffolds shown in Figure 2 C contained interconnected macro- and micropores, which were heterogeneous and isotropic. The pore wall surface texture in this scaffold was smooth and the macropore and micropore diameters ranged from 20 - 90 µm and 0.5 - 3.5 µm, respectively.

The differences in scaffold architecture can be attributed to the different mechanisms of phase separation that occurred in the different systems. In the PCL/DO solution, when the freezing point was reached, the DO crystallized and the polymer was expelled from the solvent crystallization front.²¹ The morphology of the solvent crystals dictates the pore architecture, because the pores are formed by the subsequent sublimation of the solvent and the cooling regime used has a large influence on the temperature gradient along which solvent crystallization occurs and, thereby, the

anisotropy of the formed pores. In the scaffolds produced using this solvent the slow cooling profile was used and therefore the solvent crystals grew according to the free-growth mechanism, and crystal nucleation and growth occurred randomly, leading to the observed isotropic pore architecture.^{56, 57} With the addition of the non-solvent water to the PCL/DO system, the mechanism of phase separation changed to a liquid-liquid type separation upon cooling. In the scaffolds obtained (PCL_{DO-H2O-Q} and PCL_{DO-H2O-S}), it was observed that the scaffold architecture consisted of a highly interconnected porous network leading to the inference that the system underwent a spinodal decomposition mechanism, rather than a “nucleation and growth” type phase separation under both cooling regimes used. In PCL_{DO-H2O-Q}, directionality of the structure was observed which can be attributed to a radial temperature gradient.⁵² The comparatively larger pore sizes observed in PCL_{DO-H2O-S} demonstrates that the spinodal decomposition had been followed by a coarsening stage, which is in agreement with observations made in the literature.⁵⁶⁻⁵⁸ The inclusion of water resulted in the PCL_{DO-H2O-S} system displaying a fibrous network structure. Since PCL is a semi-crystalline polymer it may have crystallised from the polymer-rich phase⁵⁹ causing the water-containing polymer-poor phase to be segregated in the locations that, after sublimation, became highly porous. This phenomenon, known as gelation, occurs at a particular temperature known as the gelation temperature⁶⁰ and has been determined to be an important factor in the formation of interconnected pores, because it can inhibit the coarsening stage, thereby reducing the formation of closed pores. Gel points have been observed in PLLA-DO-water systems,^{52, 61} although fibrous structures similar to those observed in this study have been observed in PLLA-DO-water systems without the observation of a gelation point.²¹ A gelation point was not observed in our PCL/DO/water system, however, it must be noted that the temperatures of the gel point and freezing point of the system may be similar, making it difficult to resolve them.

Fabrication and characterization of nanocomposite PCL TIPS scaffolds

Nanocomposite scaffolds were fabricated using a particle concentration of 4 g L⁻¹ for all four particle types in PCL_{DO-S} and PCL_{DO-H2O-S} scaffolds, and for HAP and HEP-A-HAP in PCL_{DO-H2O-Q} scaffolds. This resulted in composite scaffolds with a particle loading of 7.4 wt% (equivalent to 2.9 volume%) relative to PCL. The porosities of the composite scaffolds were found to fall within the range of 93 to 95 ± 1% which is similar to that observed for the pure PCL scaffolds. The mass percentage of HAP at various heights along the HAP and HEP-A-HAP scaffolds was determined in 5 mm thick slices as illustrated in Figure 3 A and the results are shown in Figure 3 B. The dotted line on the graph shows the theoretical 7.4 wt% loading level. It was observed that in all the

scaffolds a large proportion of the particles had sedimented to the bottom of the scaffold. Furthermore, there was no significant difference between the vertical distributions of the particles in any of the scaffolds examined. All scaffolds contained 2 - 5 wt% particles at a distance of 7.5 mm from the bottom and 1 - 4 wt% at the top of the scaffold (i.e., 30 - 35 mm from the bottom of the scaffold). There, thus, appears to be no effect from either the surface chemistry of the particles or the scaffold fabrication method used on the final macroscopic distribution of the particles in the vertical direction. This observation correlates with the sedimentation observed for HEP-HAP and HEP-A-HAP from the PCL/water/DO solutions, with approximately 50 % of the mass sedimenting within a 2 hour time frame (data not shown) corresponding to the time before the solutions were frozen. Based on this a loading level of approximately 3.7 wt% is expected throughout the vertical height of the scaffold, assuming that the particles are present equally throughout the scaffold and this is what is observed. Furthermore, the fact that there was no difference in the particle distribution of the composite PCL_{DO-H2O-S} scaffolds, compared to the composite PCL_{DO-H2O-Q} scaffolds indicates that the amount fully sedimenting is not dependent on how quickly the scaffold was frozen but that a certain proportion of the dried particles were present in large aggregates and these sedimented almost immediately. It is this distribution of particle sizes that remains in suspension that is determined in the DLS measurements and that are incorporated into the scaffolds.

SEM analysis of scaffold sections is displayed in Figure 2. It was observed in the composite PCL_{DO-S} scaffolds (Figure 2 F, H, J, M) that while there was no significant difference in the average pore sizes (Table 1) the incorporation of the particles affected the scaffold architecture, with a less regular structure observed compared to the PCL_{DO-S} scaffold as shown in Figure 2 C. This effect can be attributed to the perturbation caused by the particles during the solvent crystallization.²¹ In contrast, there was no significant change in the pore architecture or the pore sizes of the PCL_{DO-H2O-S} scaffolds (Figures 2 E, G, I and L and Table 1). This finding is in agreement with the predominant observation in the literature, where the addition of hydroxyapatite has been found to have little effect on the pore size or the degree of porosity of the scaffolds.^{1, 21, 28} A few studies have, however, reported changes in porosity in scaffolds with high filler content (e.g. 50 wt% HAP in PLLA composite scaffolds²⁷ and 25 wt% HAP in poly(lactic-co-glycolic acid) (PLGA) scaffolds²²). Back-scatter electron (BSE) images were recorded for HAP and HEP-A-HAP loaded PCL_{DO-S} and PCL_{DO-H2O-S} scaffolds are displayed in Figure 4. This imaging technique provides better contrast between the polymer substrate and the inorganic particles. Particle aggregates were clearly visible in the composite PCL_{DO-H2O-S} scaffolds as white areas with aggregate sizes up to 8 μm in diameter, while it was difficult to distinguish any particles in the composite PCL_{DO-S} scaffolds. This observation, however, does not correlate with the particle dispersion studies (see Figures 1 B and C)

where significantly larger HEP-A-HAP particle agglomerates were observed in the DO compared to the water/DO suspension, and this is investigated further by TEM below.

The distribution of the particles within the scaffold walls was evaluated from TEM images of 100 nm thick sections of the scaffolds taken in the regions of 0 - 5 mm, 15 - 20 mm and 30 - 35 mm from the bottom of the scaffolds. Composite PCL_{DO-S}, PCL_{DO-H₂O-S} and PCL_{DO-H₂O-Q} scaffolds incorporating HAP and HEP-A-HAP were evaluated and the TEM images of sections cut at 15 - 20 mm from the bottom are shown in Figure 5, while sections from 0 - 5 mm and 30 - 35 mm from the bottom of the scaffold are given in Supplementary Figures S6 - S8. The background grey area in the micrographs arises from the resin used in sectioning of the scaffolds. It was observed that the resin area between polymer walls was larger in PCL_{DO-S} scaffolds, compared with PCL_{DO-H₂O-S} and PCL_{DO-H₂O-Q} scaffolds which correlate with the pore sizes observed by SEM. It was observed that the particles were distributed within the scaffold walls in the PCL_{DO-S} scaffolds (Figures 5 A and B) and this was consistent across all sections evaluated. Furthermore, primary particles were observed to be well dispersed in both the HAP-PCL_{DO-S} and HEP-A-HAP-PCL_{DO-S} scaffolds despite the aggregation of the particles observed by DLS in DO suspensions. The similarity of the behaviour of the two types of particles in the scaffolds correlates with the predicted collapsed conformation of heparin in this non-polar solvent. The percentage area of the polymer covered by particles was determined in the 0 - 5 mm, 15 - 20 mm and 30 - 35 mm sections of HAP-PCL_{DO-S} to be 5 %, 3 %, 2 %, respectively. The area covered in 0 - 5, 15 - 20 and 30 - 35 mm sections of HEP-A-HAP-PCL_{DO-S} was 2 %, 1 % and 1 %, respectively. These values correlate with the bulk particle distribution described above.

TEM images of cross-sections of composite PCL_{DO-H₂O-S} scaffolds (Figures 5 C and D) revealed the particles to be embedded in the polymer to a much lower extent with percentage area of the polymer region covered by the particles at all section heights being < 0.1%. The major fraction of the particles was present in the resin and this was independent of the particle type. This observation could either be due to particles that were physically trapped within the pores or due to particles situated on the pore walls (present at the polymer-solvent interface during scaffold fabrication) and pushed out during infiltration with the resin. Overall these observations correlate with that observed in the back scatter SEM images, where particle aggregates were clearly visible in the PCL_{DO-H₂O-S} scaffolds, while it was difficult to distinguish the particles on the PCL_{DO-S} scaffolds, due to their more intimate mixing with the polymeric matrix. TEM images of cross-sections of the PCL_{DO-H₂O-Q} composite scaffolds (Figures 5 E and F) also revealed that the majority of the particles were distributed outside the scaffold walls, similar to the composite PCL_{DO-H₂O-S} scaffolds.

The observation that there was very low particle distribution within the pore walls ($< 0.1\%$ coverage of polymer area) of the PCL_{DO-H2O-S} and PCL_{DO-H2O-Q} scaffolds, while good distribution was observed within the polymer walls of the PCL_{DO-S} scaffolds does not correlate with the dispersion stability of the particles observed in solution where significantly higher stability was seen in water/DO compared with the DO suspensions. As the PCL/water/DO system underwent a liquid-liquid separation and the hydroxyapatite particles are hydrophilic, the particles may have separated into the polymer-poor water-containing phase, and during the coarsening stage, have been completely expelled from the PCL phase. However, since the particle distribution was independent of the time allowed for the coarsening to occur (e.g. both the slow and quick quench methods gave the same result) this is an unlikely explanation. Rather, the particles may have acted as an interface stabiliser and not mixed with the polymer in solution, remaining as a separate phase. This hypothesis corroborates with the fact that the surface modification of the particles did not improve the distribution of the particles in the polymer, although the study of the heparin-modified particles in water and in DO suspensions indicated that they had higher dispersion stability compared to unmodified HAP. Furthermore, it is in agreement with the lack of change in pore structure of the PCL_{DO-H2O-S} and PCL_{DO-H2O-Q} scaffolds upon inclusion of the HAP particles.

In vitro mineralisation in simulated body fluid

The mineralisation capacity of a selection of scaffolds was tested *in vitro* by investigating the deposition of calcium phosphate mineral phases on the scaffolds when immersed in SBF at 37 °C. PCL_{DO-S} and PCL_{DO-H2O-S} scaffold sections loaded with HAP and HEP-A-HAP were investigated in a 13 day study. Mass increases of between 11 and 26 % were observed in all composite scaffolds, whereas there was no change in mass in PCL_{DO-S} control scaffolds. There was no significant difference in the mass increases observed in the different composite scaffolds, and this was attributed to large errors (up to 60 %) associated with the measured mass in replicate samples. In addition, it was observed from XPS measurements that there was a large variation in the total amounts of Ca and P on the replicate samples after SBF immersion. This finding is important when considering the TEM and BSE results described above which indicated that the particles in the PCL_{DO-S} scaffolds were more intimately imbedded within the scaffold walls while the particles in the PCL_{DO-H2O-S} scaffolds were presented more on the surface of the pores. This indicates that there is sufficient surface presentation of the particles in the PCL_{DO-S} scaffolds to improve the mineralisation capacity of the PCL polymer.

Observation of the sections using SEM indicated that non-uniform apatite deposition had occurred in all composite scaffolds. An example of this can be seen in Figure 6 A which shows the variation of deposition observed in a HEP-A-HAP-PCL_{DO-H2O-S} scaffold. Higher amounts of mineral formation were observed around the edges of the specimen and little or no deposition was seen in the centre. A similar observation has been made previously for PLGA/hydroxyapatite scaffolds loaded with 25 - 45 wt% hydroxyapatite²⁴ and for PLLA and PLGA scaffolds.⁶² The observation can be explained by considering that the formed apatite nuclei on the surfaces continued to consume calcium and phosphate ions from the fluid and grow spontaneously⁶³ and so the fluid that reached the centre of the specimen was no longer super-saturated. In addition, limited diffusion of the SBF solution to the interior of the scaffold may have contributed to the non-uniform distribution. The calcium phosphate mineral that did deposit was composed of spherical nodules as shown in Figure 6 B. The morphological characteristics are similar to that observed on materials immersed in SBF reported previously.^{1, 62} XPS analysis showed that the Ca/P ratios were between 1.4 – 1.8 which is similar to that of HAP (1.67) in all samples after SBF immersion. In conclusion there was no observable difference in the mineralisation capacity or in the mineral formed regardless of the method of fabrication or particle type incorporated.

Bulk properties of the scaffolds

The compressive moduli were determined for a selection of scaffolds. It was found that there were no significant differences in the compressive moduli along the height of a PCL_{DO-S} scaffold (data not shown) and, therefore, sections for mechanical testing were cut between 5 - 10 mm from the bottom of all scaffolds tested. The compressive moduli observed are shown in Figure 7 and it can be seen that the modulus of the pristine PCL scaffolds fall within the range of 0.7 - 1.4 MPa. By taking the compressive modulus of bulk PCL ($M_n = 73000 \pm 6300$, 56 % crystalline) to be 300 MPa⁶⁴ and using the Gibson and Ashby theory for open cell foams under compression (based on an idealised open cell model in which deformation is controlled by bending of struts within the unit cell),⁶⁵ the theoretical compressive modulus of the 94 % porous PCL can be estimated to be 1.1 MPa. This value is within the range of the observed moduli of the pristine PCL scaffolds fabricated in this study. A similar compressive modulus of 1.2 MPa has previously been reported for a 88 % porous PCL scaffold prepared by TIPS.⁶⁶ The compressive modulus of the PCL_{DO-H2O-S} scaffold (comprising an isotropic fibrous structure) was significantly greater than those of the PCL_{DO-S} and PCL_{DO-H2O-Q} scaffolds ($p < 0.01$, in both cases). In the current study, the crystalline contents (X_c) of the PCL_{DO-S} and PCL_{DO-H2O-S} scaffolds, as shown in Table 1, were determined to be 74 ± 1 % and 72

± 1 %. It thus appears that it is the pore architecture which more greatly determines the mechanical properties of the scaffold.

The inclusion of particles into the scaffolds at an effective loading of 3 wt% did not significantly alter the compressive modulus in any of the types of scaffolds. As shown in Table 1, the X_c values were found to be in the range of 70 - 74 % with no significant differences between different scaffold types. This insensitivity in the bulk moduli and crystallinities for the composite PCL_{DO-H2O-S} and PCL_{DO-H2O-Q} scaffolds correlates with the majority of the particles being confined to the exterior of the walls of the scaffolds, as was evident from TEM images (see Figure 5). However, the loading of particles had no effect on the modulus in the PCL_{DO-S} scaffolds, despite the particles being observed within the bulk polymer of these samples. A previous study on hydroxyapatite/PCL composites have shown that filler inclusion as low as 5 wt% can cause an increase in the modulus of the material.²⁸ However, most studies have investigated only higher filler levels and have observed improved mechanical properties for 8 or 10 wt% loadings of filler.^{12, 28, 30, 31} In some of these studies other bulk properties also changed with added filler including reductions in porosity²⁸ and increases in crystallinity.^{12, 28, 31} Common to the materials for which an increase in crystallinity was observed was a relatively low X_c value for the polymer ranging from 38 to 50 % (i.e. lower than that of the scaffolds in the current study). The lack of change in bulk properties of PCL_{DO-S} composite scaffolds of the current study may be attributed to the filler content being below a threshold particle concentration. It has previously been concluded by Kaur et al.,⁶⁷ who used dynamic mechanical analysis on hydroxyapatite/PCL composites, that the particles interacted more with the amorphous fraction of the PCL than the crystalline regions. It is thus plausible that the hydroxyapatite particles included at relatively low filler concentrations in the amorphous regions of the polymer does not contribute significantly to either a direct mechanical strengthening or to other bulk properties such as enhanced crystallinity for polymers which are initially comprised of a high degree of crystallinity.

CONCLUSION

A thorough investigation of the dispersion stability of surface-modified and pristine HAP particles was carried out both in solution and in polymer scaffolds. It was determined that the solvent used has a significant contribution to the success of a surface modifier in improving colloidal stability in solution. Thus, the modification of HAP with heparin (by adsorption of covalent attachment via an APTES layer) improved the dispersion stability of the particles in 1 mM KCl and in a solution of PCL in mixed solvent, while no difference was produced in DO. Investigation of the distribution of

the particles within the scaffold walls and vertically in the scaffolds demonstrated that the behaviour of the particles did not mirror their behaviour in solution. Instead, it can be concluded that the polymer-solvent system used and the phase separation mechanism that occurs influences the distribution of the particles significantly. Scaffolds fabricated using a DO/water mixed solvent had the particles partitioned to the surface of the scaffold walls and this was likely because the particles acted as interface stabilisers and were not miscible in the PCL. While this could not be detected in the solution state, it is clear that it significantly changed the distribution of the particles in the scaffold. Therefore, it is not necessarily valid to predict the incorporation and distribution of filler particles in the composite scaffolds based on solution studies alone. Importantly, the use of DO as a solvent in the fabrication of composite TIPS scaffolds afforded primary particles which were well dispersed in the walls of the PCL scaffolds. The inclusion of filler particles significantly improved the mineralisation capacity in SBF compared to pristine PCL scaffolds. Despite the different particle distribution observed by TEM for the different scaffold types, there was no difference in the mineralisation outcome which indicates that the particles were present in sufficient amounts at the pore interface in all composite scaffolds prepared. For all of the scaffolds fabricated here, including those that showed good dispersion of the particles within the polymer matrix, there was no significant effect on the presence of filler particles (at a loading of 3 wt%) on bulk properties (compressive modulus, crystalline content or glass transition temperature). This lack of enhancement in bulk mechanical properties of the PCL scaffolds which possess relatively high crystallinity (70-74%) may be attributed to the particles being present in the amorphous phase of the polymer and therefore having little effect on the overall modulus of the scaffolds.

ACKNOWLEDGEMENTS

This work was carried out in part at the Centre for Microscopy and Microanalysis, The University of Queensland node of the Australian Microscopy and Microanalysis Research Facility (AMMRF). C.S.G. would like to thank the Australian government and the University of Queensland for awarding an International Postgraduate Research Scholarship and a UQ Research Scholarship.

REFERENCES

1. K. S. Jack, S. Velayudhan, P. Luckman, M. Trau, L. Grøndahl and J. Cooper-White, *Acta Biomater.*, 2009, **5**, 2657-2667.
2. Y. Cui, Y. Liu, X. B. Jing, P. B. A. Zhang and X. S. Chen, *Acta Biomater.*, 2009, **5**, 2680-2692.
3. W. Han, J. Zhao, M. Tu, R. Zeng, Z. Zha and C. Zhou, *J. Appl. Polym. Sci.*, 2013, **128**, 1332-1338.
4. D. W. Schaefer and R. S. Justice, *Macromolecules*, 2007, **40**, 8501-8517.
5. M. Wang and W. Bonfield, *Biomaterials*, 2001, **22**, 1311-1320.

6. H. L. Nichols, N. Zhang, J. Zhang, D. Shi, S. Bhaduri and X. Wen, *J. Biomed. Mater. Res., Part A*, 2007, **82A**, 373-382.
7. H. J. Lee, H. W. Choi, K. J. Kim and S. C. Lee, *Chem. Mater.*, 2006, **18**, 5111-5118.
8. X. Y. Qiu, L. Chen, J. L. Hu, J. R. Sun, Z. K. Hong, A. X. Liu, X. S. Chen and X. B. Jing, *J. Polym. Sci., Part A: Polym. Chem.*, 2005, **43**, 5177-5185.
9. B. Rai, W. Noohom, P. H. Kithva, L. Grøndahl and M. Trau, *Chem. Mater.*, 2008, **20**, 2802-2808.
10. W. Noohom, K. S. Jack, D. Martin and M. Trau, *Biomed. Mater.*, 2009, **4**, 015003.
11. X. Qiu, Z. Hong, J. Hu, L. Chen, X. Chen and X. Jing, *Biomacromolecules*, 2005, **6**, 1193-1199.
12. G. Fu, L. Zeng, J. Jiang, Z. Xia, B. Jing and X. Zhang, *Polym. Polym. Compos.*, 2012, **20**, 463-469.
13. Z. Hong, P. Zhang, C. He, X. Qiu, A. Liu, L. Chen, X. Chen and X. Jing, *Biomaterials*, 2005, **26**, 6296-6304.
14. Y. Dai, M. Xu, J. Wei, H. Zhang and Y. Chen, *Appl. Surf. Sci.*, 2012, **258**, 2850-2855.
15. J. C. Wei, A. X. Liu, L. Chen, P. B. Zhang, X. S. Chen and X. B. Jing, *Macromol. Biosci.*, 2009, **9**, 631-638.
16. H. W. Choi, H. J. Lee, K. J. Kim, H. M. Kim and S. C. Lee, *J. Colloid Interface Sci.*, 2006, **304**, 277-281.
17. J. Zhang, M. Maeda, N. Kotobuki, M. Hirose, H. Ohgushi, D. Jiang and M. Iwasa, *Mater. Chem. Phys.*, 2006, **99**, 398-404.
18. B. Rai, L. Grøndahl and M. Trau, *Langmuir*, 2008, **24**, 7744-7749.
19. C. S. Goonasekera, K. S. Jack, G. Bhakta, B. Rai, E. Luong-Van, V. Nurcombe, S. M. Cool, J. J. Cooper-White and L. Grøndahl, *Biointerphases*, 2015, (accepted).
20. M. Xanthos, in *Functional Fillers for Plastics*, ed. M. Xanthos, Wiley-VCH Verlag GmbH & Co. KGaA, 2005, pp. 1-16.
21. G. Wei and P. X. Ma, *Biomaterials*, 2004, **25**, 4749-4757.
22. Y. X. Huang, J. Ren, C. Chen, T. B. Ren and X. Y. Zhou, *J. Biomater. Appl.*, 2008, **22**, 409-432.
23. L. Chen, C. Y. Tang, C. P. Tsui and D. Z. Chen, *J. Mech. Behav. Biomed. Mater.*, 2013, **22**, 41-50.
24. N. Aboudzadeh, M. Imani, M. A. Shokrgozar, A. Khavandi, J. Javadpour, Y. Shafieyan and M. Farokhi, *J. Biomed. Mater. Res., Part A*, 2010, **94A**, 137-145.
25. M. P. Prabhakaran, J. Venugopal and S. Ramakrishna, *Acta Biomater.*, 2009, **5**, 2884-2893.
26. Y. W. Wang, Q. Wu, J. Chen and G. Q. Chen, *Biomaterials*, 2005, **26**, 899-904.
27. X. Wang, G. Song and T. Lou, *Med. Eng. Phys.*, 2010, **32**, 391-397.
28. Y. Wang, J. Dai, Q. Zhang, Y. Xiao and M. Lang, *Appl. Surf. Sci.*, 2010, **256**, 6107-6112.
29. X. Xu, X. Chen, A. Liu, Z. Hong and X. Jing, *Eur. Polym. J.*, 2007, **43**, 3187-3196.
30. D. O. Costa, S. J. Dixon and A. S. Rizkalla, *ACS Appl. Mater. Interfaces*, 2012, **4**, 1490-1499.
31. J. Hao, M. Yuan and X. Deng, *J. Appl. Polym. Sci.*, 2002, **86**, 676-683.
32. M. Chen, J. Yin, X. Liu, Y. Feng, B. Su and Q. Lei, *Thin Solid Films*, 2013, **544**, 116-119.
33. J. Meeus, X. Chen, D. J. Scurr, V. Ciarnelli, K. Amssoms, C. J. Roberts, M. C. Davies and G. v. Den Mooter, *J. Pharm. Sci.*, 2012, **101**, 3473-3485.
34. P. Salmon and A. Sasov, in *Advanced Bioimaging Technologies in Assessment of the Quality of Bone and Scaffold Materials*, eds. L. Qin, H. Genant, J. Griffith and K. Leung, Springer Berlin Heidelberg, 2007, pp. 323-331.
35. C. Albano, G. González, J. Palacios, A. Karam and M. Covis, *Polym. Compos.*, 2013, **34**, 1433-1442.
36. P. Rittigstein, R. D. Priestley, L. J. Broadbelt and J. M. Torkelson, *Nat. Mater.*, 2007, **6**, 278-282.

37. S. I. J. Wilberforce, C. E. Finlayson, S. M. Best and R. E. Cameron, *Polymer*, 2011, **52**, 2883-2890.
38. N. Klein, G. Marom and E. Wachtel, *Polymer*, 1996, **37**, 5493-5498.
39. T. Kokubo and H. Takadama, *Biomaterials*, 2006, **27**, 2907-2915.
40. S. M. Cool, B. Kenny, A. Wu, V. Nurcombe, M. Trau, A. I. Cassady and L. Grondahl, *J. Biomed. Mater. Res., Part A*, 2007, **82A**, 599-610.
41. K. Søballe and S. Overgaard, *J. Bone Joint Surg. Brit.*, 1996, **78-B**, 689-691.
42. K. Søballe, E. S. Hansen, H. Brockstedt-Rasmussen and C. Bunger, *J. Bone Joint Surg. Brit.*, 1993, **75-B**, 270-278.
43. C. S. Goonasekera, K. S. Jack, J. J. Cooper-White and L. Grondahl, *J. Mater. Chem. B*, 2013, **1**, 5842-5852.
44. W. S. Rasband, U. S. National Institutes of Health, Bethesda, Maryland, USA, 1997-2012.
45. G. With, H. J. A. Dijk, N. Hattu and K. Prijs, *J. Mater. Sci.*, 1981, **16**, 1592-1598.
46. K. Van de Velde and P. Kiekens, *Polym. Test.*, 2002, **21**, 433-442.
47. V. Crescenzi, G. Manzini, G. Calzolari and C. Borri, *Eur. Polym. J.*, 1972, **8**, 449-463.
48. Y. Han, X. Wang and S. Li, *J. Nanopart. Res.*, 2009, **11**, 1235-1240.
49. E. Luong-Van, L. Grøndahl, K. N. Chua, K. W. Leong, V. Nurcombe and S. M. Cool, *Biomaterials*, 2006, **27**, 2042-2050.
50. F. J. Tsai and J. M. Torkelson, *Macromolecules*, 1990, **23**, 775-784.
51. P. van de Witte, P. J. Dijkstra, J. W. A. van den Berg and J. Feijen, *J. Membr. Sci.*, 1996, **117**, 1-31.
52. Y. S. Nam and T. G. Park, *J. Biomed. Mater. Res.*, 1999, **47**, 8-17.
53. Y. Cao, G. Mitchell, A. Messina, L. Price, E. Thompson, A. Penington, W. Morrison, A. O'Connor, G. Stevens and J. Cooper-White, *Biomaterials*, 2006, **27**, 2854-2864.
54. P. A. George, K. Quinn and J. J. Cooper-White, *Biomaterials*, 2010, **31**, 641-647.
55. Y. Cao, T. I. Croll, A. J. O'Connor, G. W. Stevens and J. J. Cooper-White, *J. Biomater. Sci., Polym. Ed.*, 2006, **17**, 369-402.
56. Y. S. Nam and T. G. Park, *Biomaterials*, 1999, **20**, 1783-1790.
57. S.-W. Song and J. M. Torkelson, *Macromolecules*, 1994, **27**, 6389-6397.
58. L. He, Y. Zhang, X. Zeng, D. Quan, S. Liao, Y. Zeng, J. Lu and S. Ramakrishna, *Polymer*, 2009, **50**, 4128-4138.
59. P. X. Ma and R. Zhang, *J. Biomed. Mater. Res.*, 1999, **46**, 60-72.
60. C. A. Martínez-Pérez, I. Olivás-Armendariz, J. S. Castro-Carmona and P. E. García-Casillas, in *Advances in Regenerative Medicine*, ed. S. Wislet-Gendebien, InTech, 2011, pp. 275-294.
61. F. J. Hua, G. E. Kim, J. D. Lee, Y. K. Son and D. S. Lee, *J. Biomed. Mater. Res.*, 2002, **63**, 161-167.
62. R. Zhang and P. X. Ma, *Macromol. Biosci.*, 2004, **4**, 100-111.
63. H.-M. Kim, T. Himeno, M. Kawashita, T. Kokubo and T. Nakamura, *J. R. Soc. Interface*, 2004, **1**, 17-22.
64. S. Eshraghi and S. Das, *Acta Biomater.*, 2010, **6**, 2467-2476.
65. L. J. Gibson and M. F. Ashby, *Cellular Solids: Structure and Properties*, Cambridge University Press, Cambridge, UK, 1997.
66. J. Z. Luk, J. Cooper-White, L. Rintoul, E. Taran and L. Grondahl, *J. Mater. Chem. B*, 2013, **1**, 4171-4181.
67. J. Kaur and M. L. Shofner, *Macromol. Chem. Phys.*, 2009, **210**, 677-688.

Tables

Table 1. Pore sizes determined for the scaffolds and X_c values measured for the selected scaffolds (determined using sections taken at 30 - 35 mm from the bottom of the scaffold)

Scaffold	Macropore diameter (μm)	X_c (%)
PCL _{DO-S}	20 - 90	73.5 \pm 1.3
HAP-PCL _{DO-S}	10 - 80	70.3 \pm 1.5
A-HAP-PCL _{DO-S}	10 - 80	–
HEP-HAP-PCL _{DO-S}	20 - 90	–
HEP-A-HAP-PCL _{DO-S}	5 - 110	71.9 \pm 1.0
PCL _{DO-H2O-S}	3 - 50	71.4 \pm 1.4
HAP-PCL _{DO-H2O-S}	10 - 50	72.3 \pm 0.9
A-HAP-PCL _{DO-H2O-S}	10 - 50	–
HEP-HAP-PCL _{DO-H2O-S}	15 - 60	–
HEP-A-HAP-PCL _{DO-H2O-S}	10 - 60	70.4 \pm 2.2

Figures

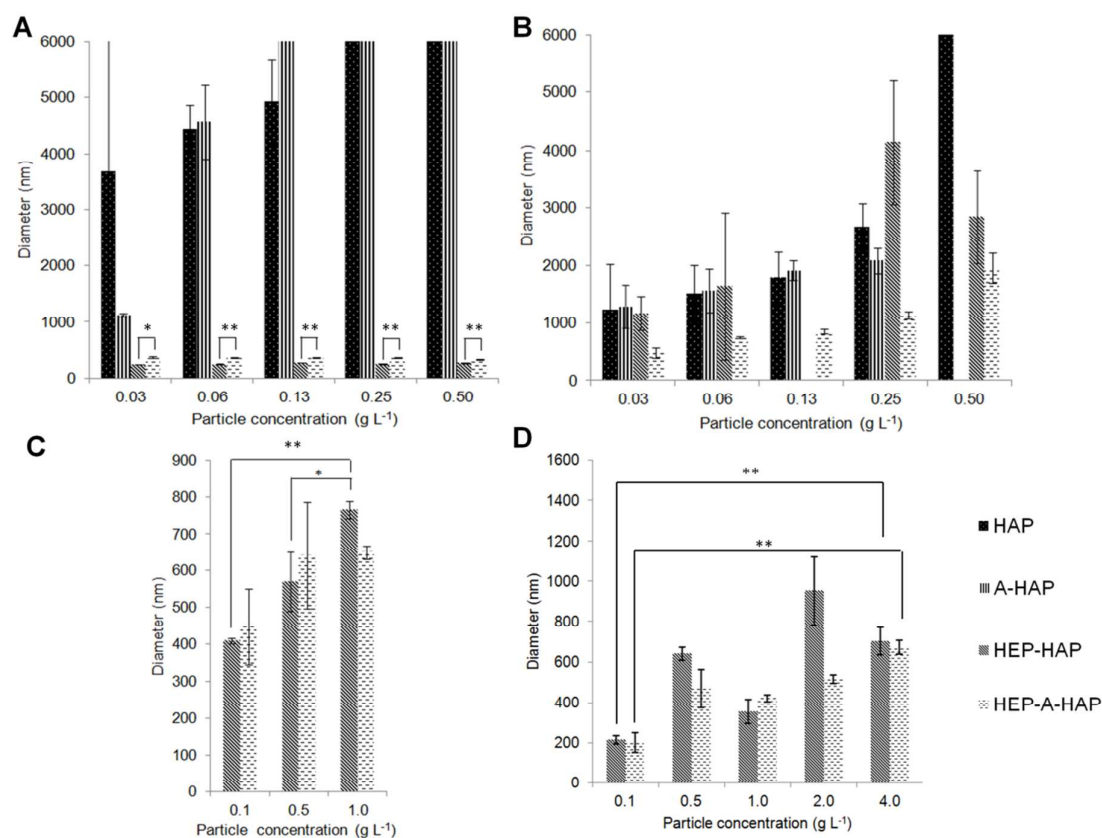


Figure 1. Particle diameters observed at different particle concentrations, 15 minutes after dispersion in (A) 1 mM KCl, (B) DO, (C) 5 % (v/v) water/DO and (D) PCL/water/DO (the error bars represent standard deviations, $n = 3$, $*p < 0.05$, $**p < 0.01$). The ordinate axes of A and B have been truncated at 6000 nm as this represents the maximum size that can be accurately measured by this technique.

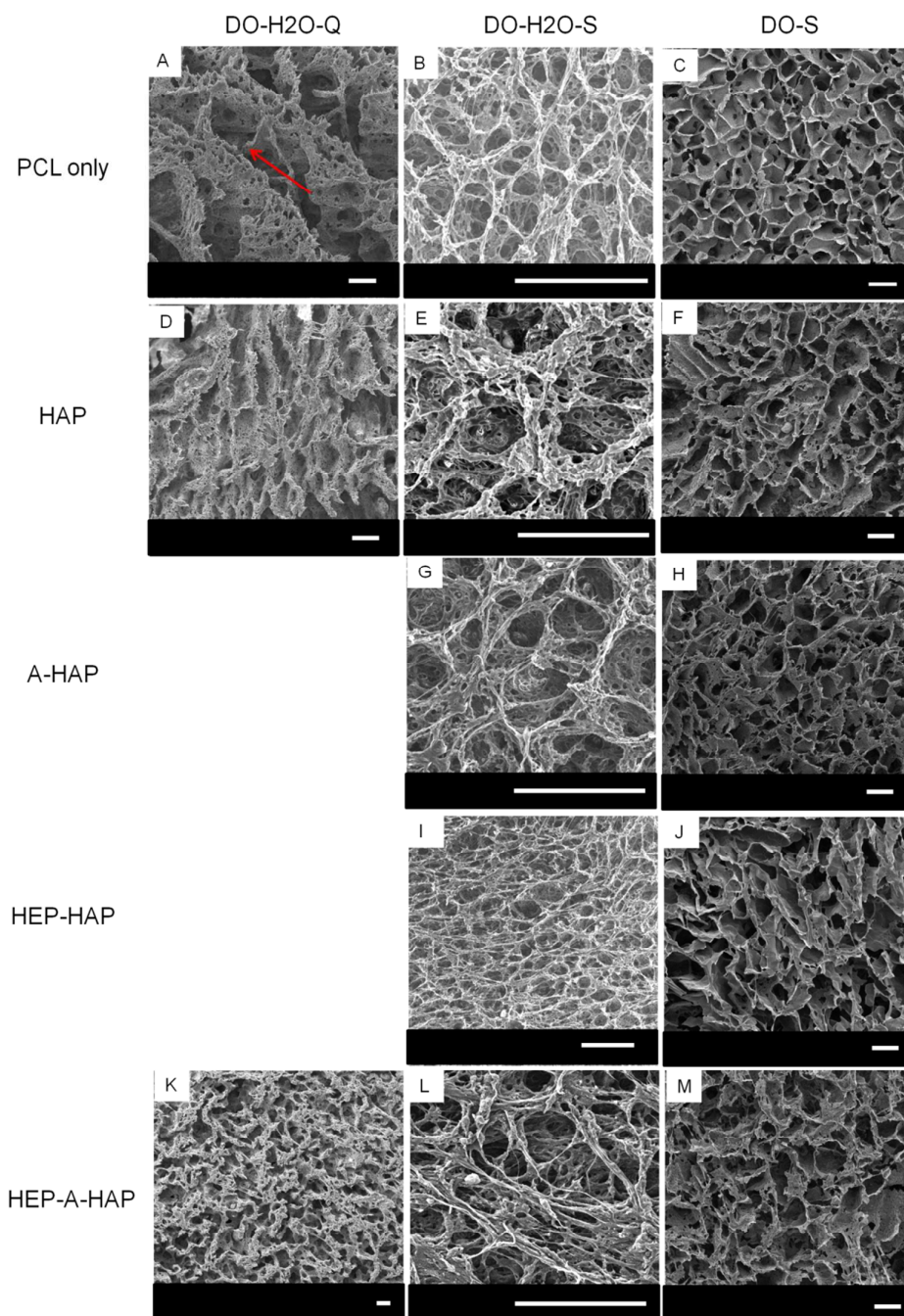


Figure 2. SEM images taken from cross-sections of PCL scaffolds and HAP, A-HAP, HEP-HAP and HEP-A-HAP composite scaffolds fabricated in water/DO using the quick-quench cooling profile (Column 1), in water/DO using the slow-quench cooling profile (Column 2) and in DO using the slow-quench cooling profile (Column 3). For the composite scaffolds, the scaffold slices were obtained at 15 - 20 mm from bottom of the scaffolds (the scale bars = 100 μ m in all images).

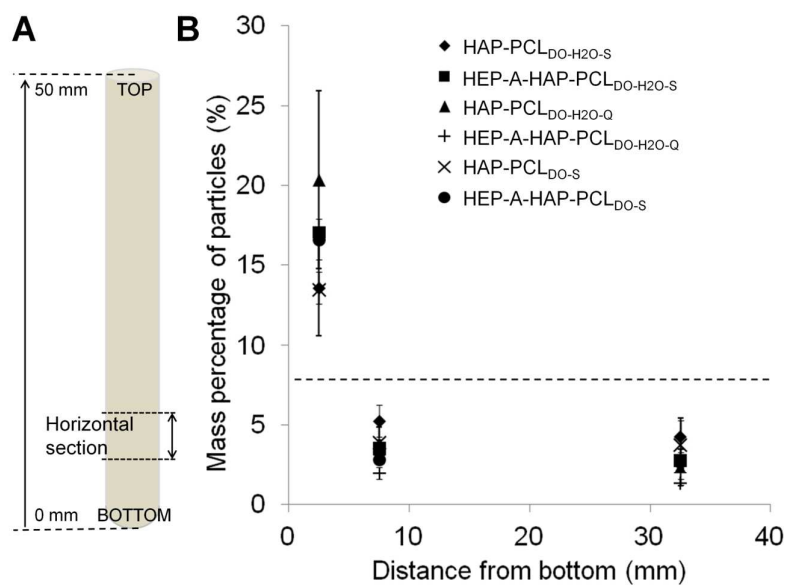


Figure 3. (A) Diagrammatic representation of a fabricated scaffold and positioning of horizontal sections and (B) the vertical distributions of the particles in the scaffolds, as determined using a Ca ion selective electrode. The dotted line on the graph shows the theoretical 7.4 wt% loading level (the error bars represent standard deviations, $n = 3$).

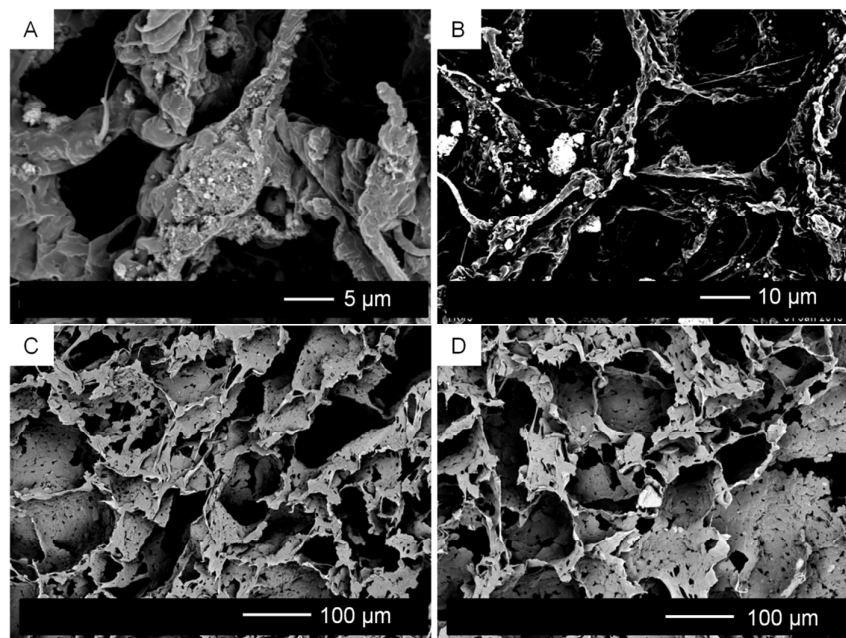


Figure 4. Back-scatter SEM images of (A) HAP-PCL_{DO-H2O-S}, (B) HEP-A-HAP-PCL_{DO-H2O-S}, (C) HAP-PCL_{DO-S} and (D) HEP-A-HAP-PCL_{DO-S}. The scaffold slices used for imaging were obtained at 15 - 20 mm from bottom of the scaffolds.

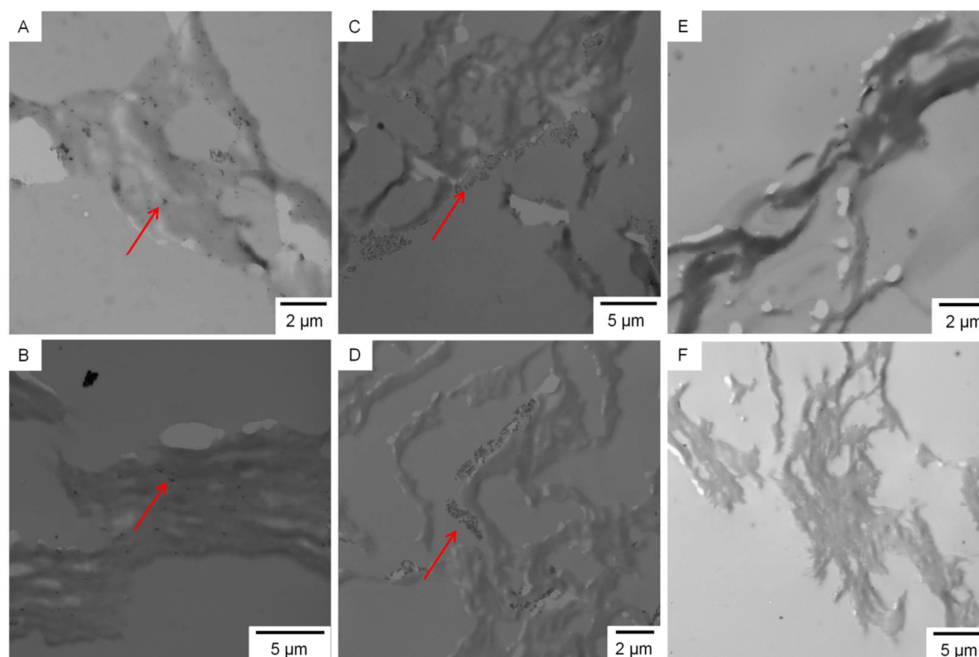


Figure 5. TEM images of (A) HAP-PCL_{DO-S}, (B) HEP-A-HAP-PCL_{DO-S}, (C) HAP-PCL_{DO-H2O-S}, (D) HEP-A-HAP-PCL_{DO-H2O-S}, (E) HAP-PCL_{DO-H2O-Q} and (F) HEP-A-HAP-PCL_{DO-H2O-Q}, sections taken 15 - 20 mm from the bottom of the scaffold. The arrows show the regions in which the particles are observable.

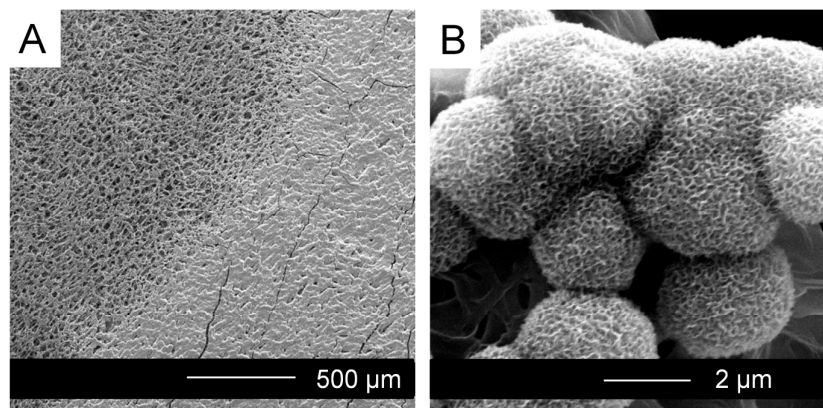


Figure 6. Mineral deposition after immersion of HEP-A-HAP-PCL_{DO-H2O-S} in SBF: (A) a lower resolution image showing variation in mineral deposit on the scaffold and (B) a higher magnification image of the mineral deposit. Sections were taken from 15 - 20 mm from the bottom of the scaffold.

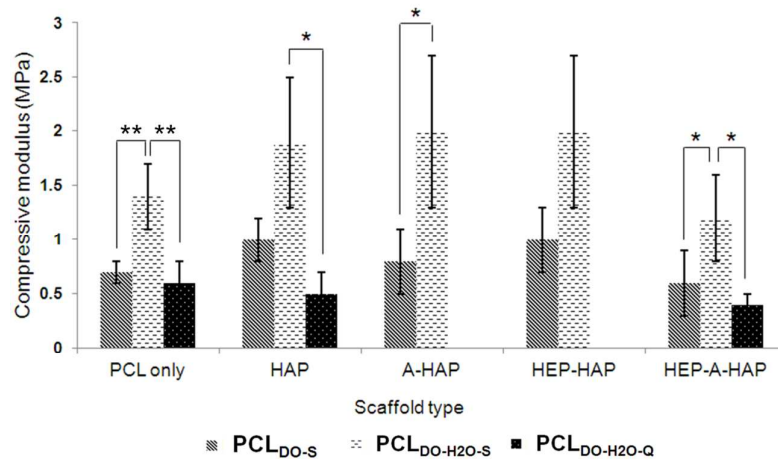
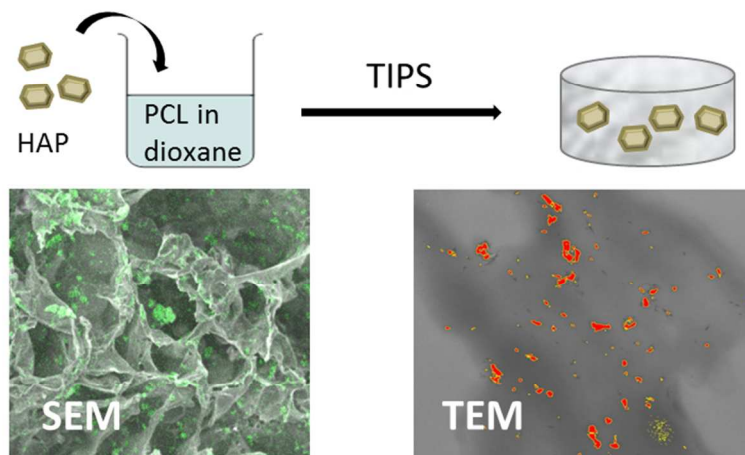


Figure 7. Compressive moduli measured for the scaffolds (the error bars represent standard deviations, $n = 3 - 5$, $*p < 0.05$, $**p < 0.01$)



79x39mm (300 x 300 DPI)